AN AAM-BASED DETECTION APPROACH OF LUNG NODULES FROM LDCT SCANS

Amal Farag[1], *Hossam Abdelmunim*[1,2], *James Graham*[1], *Aly A. Farag*[1], *Cambron Carter*[1],
Salwa Elshazly[1], Mohamed S. El-Mogy[3], Sabry El-Mogy[3,4], and Robert Falk[5]

[1]Computer Vision and Image Processing Laboratory (CVIP Lab),
University of Louisville, Louisville KY 40292.
[2]Computer & Systems Engineering Department, Faculty of Engineering,
Ain Shams University, Cairo 11517, Egypt.
[3]Mogy Scan Center, Mansoura, Egypt.
[4]School of Medicine, Mansoura University, Egypt.
[5]Jewish Hospital and 3DR, Louisville, Kentucky.

ABSTRACT

In this, paper a new approach for lung nodules detection from LDCT scans is proposed. Intensity models of the nodules are generated using an active appearance model formulation. Template matching is used to compute a similarity score between the AAM template and the input image. The goal is to maximize the similarity measure at different image pixels to increase nodule detection. Conventional template matching does not account for rotation variations. Our proposed template matching approach is formulated as an energy optimization problem that computes a transformation that includes rotation(s) parameters as well as the AAM weighting coefficients. The approach is flexible to different scans and different nodule locations because of the ability to handle the variations in the rotation between the template and the input images. The approach can employ different similarity measures. Experimental results will be shown using three similarity measures from the literature: NCC, ZNCC and ZSSD; which illustrate the efficiency of the proposed approach. ROC curves for various nodule types are constructed on a clinical study with known ground truth, showing significant enhancements over conventional parametric nodule models and traditional template matching criterion.

1. INTRODUCTION

Computer-Assisted Diagnosis (CAD) of lung nodules from low dose CT (LDCT) scans of the human chest is an active area of research (e.g.,[7][5]). Fig.1 illustrates the components of a typical CAD system. Our efforts (e.g., [8], [3], [9]) created and tested several approaches for lung tissue segmentation and nodule detection. This paper deals with nodule detection and the role of data in devising nodule models that capture the physical characteristics of lung nodules as seen by a radiologist. From an image analysis prospectives, nodules possess various uncertainties in the modeling process due to size, contrast, shape, and occlusion - our focus has been on early detection; i.e., with small nodules of 1cm or less, resembling spatial supports of 5-10 pixels in a typical slice from a LDCT chest scan. Such uncertainties provide a real challenge for CAD models in terms of training, testing and validation. Our experience showed the promise of shape and appearance models, developed in the computer vision literature, (e.g., [2], [4]) in lung nodule modeling. Using the active appearance models (AAM) to model the lung nodules has been shown to lend higher sensitivity and specificity over parametric models (e.g., [3], [9]). This paper provides further enhancements for lung nodule modeling using the AAM approach, evaluates the performance on a clinical study, shows the ROC for various nodule types, as an attempt to answer the following question: *how far early detection of lung nodules from LDCT scans can go with respect to human experts?*. In this, paper we examine the usage of the eigennodules generated from the principle component analysis (PCA) process undergone after alignment of the training shapes versus the usage of one average template per nodule type. The eigennodules generated by enforcing a PCA criterion generates multiple model variations pertaining to each nodule type from the ensemble of categorized nodules, thus, multiple templates are used in the detection process. In the literature the well-known template matching using zero-mean normalized cross-correlation (ZNCC) and normalized-cross correlation(NCC) similarity measures are typically used for lung nodule detection. In this, paper a new formulation to the typical template matching approach is formulated taking into account rotations variations between the template and input images with an optimizer in the form of the Gradient descent method. The similarity correlation measures are also not limited to just the zero mean normalized-cross correlation (ZNCC) and normalized-cross correlation (NCC), but also uses the Zero-mean Sum of Squared Differences(ZSSD) for analysis.

2. LUNG NODULES MODELING

In a CT of the lung a pulmonary nodule usually appears as a spherically shaped mass; however, this mass can be distorted by the pleural surface and surrounding anatomical structures. The classification of Kostis et al. ([1]) is adopted in this paper, which groups the lung nodules into four classes: juxta-pleural where a significant portion of the nodule is connected to the pleural surface; vascularized where the nodule has significant connection(s) to the neighboring vessels while located centrally in the lung; well-circumscribed where the nodule is located centrally in the lung without being connected to vasculature; and pleural tail where the nodule is near the pleural surface, connected by a thin structure; In all of these types there is no limitations on size or distribution in the lung tissue.

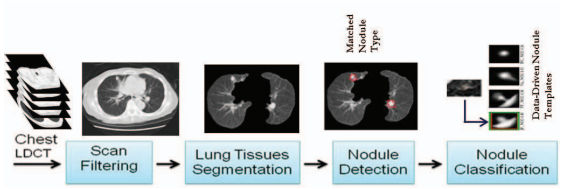


Fig. 1. A block diagram of the major steps involved in computer-based analysis of LDCT of the chest in order to detect and classify doubtful lung nodules.

A database of 96 pre-identified nodules (24 nodules per type) by a bounding box of size 21x21 pixels (this region is based on the radial distance distribution) was constructed in [9], using a semi-automatic method of cropping and categorizing each nodule into one of the four nodule types. These 24 nodules per type were annotated to highlight the basic geometric and structural features of the nodules. Let the annotated database of n nodule types be represented as $T = \{G_1, G_2, ..., G_n\}$ where each $G_n = \{s_1^n, s_2^n, ..., s_k^n\}$ where $s_k^n : R2 \rightarrow R$ represents the sample nodule annotated image. In this work, $n = 4$ and $k = 24$. These images are aligned by employing the Procrustes approach [10], thus producing n sets of aligned images where, $\tilde{T} = \{\tilde{G_1}, \tilde{G_2}, ..., \tilde{G_n}\}$. The average nodule image for each $\tilde{G_n}$ is computed as $\bar{s}^n = (\frac{1}{k})\sum(\tilde{s_k}^n)$. For any set of nodule images indexed by i, its image deviations from its mean are $\{\bar{G}_1^i = \tilde{s_1}^i - \bar{s}^i, \bar{G}_2^i = \tilde{s_2}^i - \bar{s}^i, ..., \bar{G}_k^i = \tilde{s_k}^i - \bar{s}^i\}$ where each image is of size $N_1 \times N_2$. Each image is converted into a column vector by taking row by row and setting them together as a one dimensional matrix Ξ. We form the matrices $S_i = [\Xi_1^i \Xi_2^i ... \Xi_k^i]$ and $\Psi = \frac{1}{k} S_i S_i^T$. An eigenvalue decomposition is employed to factor the matrix Ψ as $\Psi = U \sum U^T$ where U is an $N \times k$ matrix where $N = N_1 \times N_2$. Each column vector of the matrix U indexed by j is converted into a two dimensional image $\hat{s}_j^i$. From these eigen images, we can formulate an active appearance model of the nodule set images i as $AAM_i = \bar{s}^i + \sum_{j=1}^m w_j \hat{s}_j^i$ where $w_j \in R$. The number m is the number of modes to consider. From this model we can build nodule training images as $I_j^i = \bar{s}^i + \hat{s}_j^i$. The number of modes can be computed from the relation: $\sum(_{z=1}^m)\lambda_z \geq \frac{r}{100}\sum(_{z=1}^k \lambda_z)$ where $r = 97\%$, and $[\lambda_z]$ are the non zero eigen values. This will result in an average of $m = 5$ eigen images, i.e. eigennodules, per nodule type to be generated, for usage as the templates in the detection process. Average nodule image of each set of the four nodule types is shown in Fig. 2.

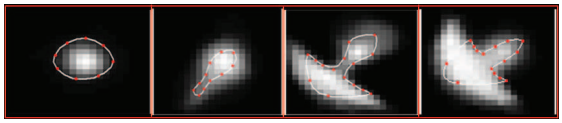


Fig. 2. Nodule models using the mean shape and texture of co-registered nodules. The resultant nodule models are based on the average of shape and texture from the AAM approach (e.g., [9]). From right to left the respective nodule representations are: Well-circumscribed, vascularized, pleural-tail and juxta-pleural.

3. TEMPLATE MATCHING AND REGISTRATION

Assume a template image $I_t : \Omega_t \subset R^2 \rightarrow R$ and an input image $I_i : \Omega_i \rightarrow R$, the zero-mean normalized cross correlation (ZNCC) between the two images is defined as:

$$\xi(\mathbf{X}_i) = \frac{\int_{\Omega_t}(I_t(\mathbf{X}_t) - \mu_t)(I_i(\mathbf{X}_t + \mathbf{X}_i) - \mu_i)d\Omega_t}{\sqrt{\int_{\Omega_t}(I_t(\mathbf{X}_t) - \mu_t)^2 d\Omega_t \int_{\Omega_t}(I_i(\mathbf{X}_t + \mathbf{X}_i) - \mu_i)^2 d\Omega_t}} \quad (1)$$

where $\mathbf{X}_i \in \Omega_i$, $\mathbf{X}_t \in \Omega_t$, the template image average is $\mu_t = \frac{\int_{\Omega_t} I_t(\mathbf{X}_t)d\Omega_t}{\int_{\Omega_t} d\Omega_t}$, and the corresponding space intensity average in the input image is defined as $\mu_i = \frac{\int_{\Omega_t} I_i(\mathbf{X}_t + \mathbf{X}_i)d\Omega_t}{\int_{\Omega_t} d\Omega_t}$. We assume the functional $\varphi : R^2 \rightarrow R$ such that for any two images I_1 and I_2, the function is written as $\varphi(I_1, I_2) = \int_{\Omega_1}(I_1(\mathbf{X}_1) - \mu_1)(I_2(\mathbf{X}_1 + \mathbf{X}_2) - \mu_2)d\Omega_1$ where the average parameters and image domains are defined as above. Now, the above similarity measure can be written as:

$$\xi(\mathbf{X}_i) = \frac{\varphi(I_t(\mathbf{X}_t), I_i(\mathbf{X}_t + \mathbf{X}_i))}{\sqrt{\varphi(I_t(\mathbf{X}_t), I_t(\mathbf{X}_t))\varphi(I_i(\mathbf{X}_t + \mathbf{X}_i), I_i(\mathbf{X}_t + \mathbf{X}_i))}} \quad (2)$$

Our goal is to maximize such a similarity measure over the whole domain of the input image Ω_i. Using the template image as is will have limited results on that measure especially when the problem encounters rotations variations. So, we incorporate a geometric transformation process on the template image such that the parameters of that transformation are selected to maximize the similarity ξ_i. Assume a geometric transformation function $\mathbf{A}(\mathbf{X}_t) = \mathbf{R}\mathbf{X}_t$ where $\mathbf{R}$ is the

rotation matrix. For each point $\mathbf{X}_i$, there exists a geometric transformation $\mathbf{A}_i$ that maximizes the ZNCC similarity measure. The similarity measure is re-written after incorporating the transformation as:

$$\xi(\mathbf{X}_i) = \frac{\varphi(I_t(\mathbf{X}_t), I_i(\mathbf{A}_i + \mathbf{X}_i))}{\sqrt{\varphi(I_t(\mathbf{X}_t), I_t(\mathbf{X}_t))\varphi(I_i(\mathbf{A}_i + \mathbf{X}_i), I_i(\mathbf{A}_i + \mathbf{X}_i))}} \quad (3)$$

Using the AAM shown above, the template function is expressed in terms of the weighted eigen shapes $I_t = \overline{I} + \sum_{j=1}^{m} w_j I_j$. The transformation parameters as well as N-weighting coefficients are required to maximize the similarity measure. The gradient descent approach is used in this optimization problem.

Summarizing the above approach: for every point in the input image domain, a ZNCC similarity measure is computed after finding the corresponding weighting coefficients and transformation parameters that maximizes such a criteria. Local maxima points are determined by a thresholding criteria to find the best matches. The above formulation can be derived for other similarity measures (ZSSD, NCC, ...etc.) in a straightforward manner.

4. RESULTS

Studies in this paper are based on the ELCAP public database [6], which contains 50 sets of LDCT lung scans taken at a single breath-hold with slice thickness 1.25 mm. The locations of the 397 nodules are provided by the radiologists, where 39.12% are juxta-pleural nodules, 13.95% are vascularized nodules, 31.29% are well-circumscribed nodules and 15.65% are pleural-tail nodules. The ELCAP database is of resolution $0.5mm \times 0.5mm$ [6]. In the first set of experimentations conducted, the four average and eigennodule templates are used in the detection process using template matching without any rotation or scale variations. The three correlation similarity measures were employed in the detection process using the average nodule templates. The receiver operating characteristic curve (ROC) and computed area under curve (AUC) for each similarity measure is shown in Fig. 3. The detection process shows the ZSSD correlation measure provided the best results while the ZNCC showed the poorest detection results with respect to the other methods employed. The NCC out-performed its zero-mean counterpart, ZNCC, in the detection results when compared to one another. The ZSSD computation relies on the squared differences followed by the aggregation between the pixels within a square neighborhood between the template image and the image slice. Since, the training data for the lung nodule modeling process and the testing is conducted on the same low-dose CT (LDCT) datasets the out-performance of detection using ZSSD can be validated. The ROC results in Fig. 4 shows the usage of the eigennodule templates with ZSSD, NCC and ZNCC correlation similarity measures in the detection process. Variations in the computed AUC for the ROC curves shown in Fig. 4 between the three methods are relatively smaller than the variations seen when the average nodule templates were used for detection.

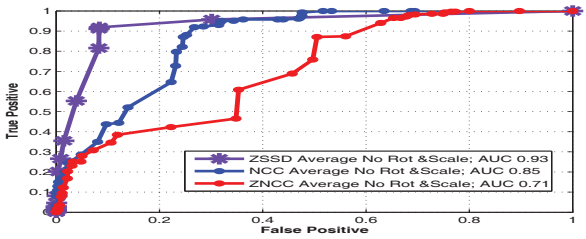


Fig. 3. ROC curve for template matching detection without rotation using the four average nodule templates and three correlation similarity measures. Computed area under curve for the detection process using each similarity measure is shown.

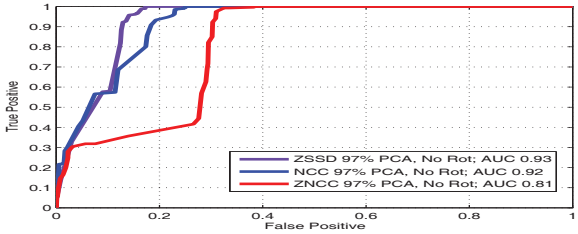


Fig. 4. ROC curve for template matching detection without rotation using the five eigennodule templates per nodule type (i.e. 20 total models) and three different correlation similarity measures. Computed area under curve for the detection process using each similarity measure is shown.

Several conclusions can be made from the curves, first using the eigen nodule templates provided better results with the NCC and ZNCC similarity measures employed in the template matching. Secondly, with false positive rate 10% the ZSSD using the average nodule templates provides above 90% true positive nodule detection rate this performance level is reached by the NCC using the average templates when the false positive rate is 30%. The results for the ZSSD using the eigennodules and average nodule templates provided the best AUC computed rates when compared to the other similarity measures at 0.93. Experimentations on the rotation template matching using the average and eigennodule templates are depicted in Fig. 6 and Fig. 5. The experiments depicted showed overall improvements in detection using either sets of the generated nodule templates. The ZNCC similarity measure with rotation template matching using both the average and eigennodules provided the most improvements in detection rates as can be inferred by the AUC computations.

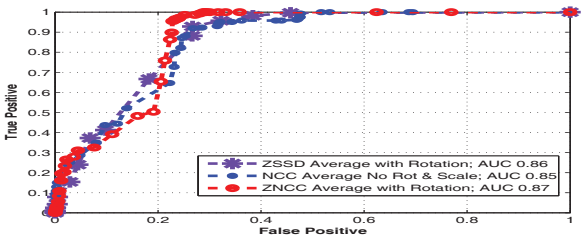


Fig. 5. ROC comparison using the average templates for lung nodule detection with rotation and three different correlation similarity measures.

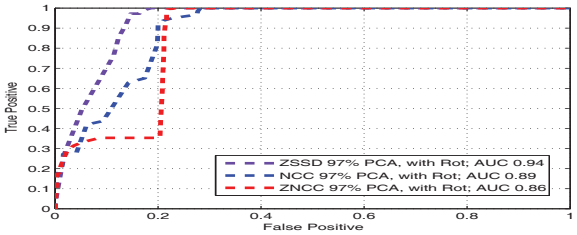


Fig. 6. ROC comparison between the eigen nodules with rotation involvement and three different correlation similarity measures.

5. CONCLUSION

In this paper a new detection approach using template matching for lung nodule detection incorporating AAM templates with rotations was formulated. The detection approach is represented as an energy optimization function to be maximized for detecting and localizing nodules. Similarity measures over the whole image domain are used to define the local maxima positions of the lung nodules. The formulated approach is flexible to various similarity measures and databases. Also, the optimization process is able to successfully compute the rotations and AAM parameters at different image pixels positions. Through the experimentations, it is seen that the embedding of rotation variations improves the template matching detection results and provides better true positive detection. Incorporating scale invariant features in the detection process is still an open issue especially with small spatial support regions, which needs further investigation. Also, implementation using sophisticated GPUs techniques can expedite the performance.

Acknowledgements: This research has been funded by the Kentucky Lung Cancer Program. Data and expertise from Mogy Scan, Mansoura, Egypt, 3DR and Jewish Hospital, Louisville, KY and Ain Shams University, Egypt are greatly appreciated.

6. REFERENCES

[1] W.J. Kostis, A.P. Reeves, D. F. Yankelevitz and C. I. Henschke. "Three dimensional segmentation and growth-rate estimation of small pulmonary nodules in helical CT images." Medical Imaging IEEE Transactions. 2003. Vol. 22. pp. 1259-1274.

[2] T.F. Cootes, G.J. Edwards, C.J. Taylor, "Active Apperance Models." IEEE Transactions on Pattern Analysis and Machine Intelligence. Vol. 23. Issue 6. 2001 pp. 681-685.

[3] Amal A. Farag, S.Y. Elhabian, S.A. Elshazly and A.A. Farag, "Quantification of Nodule Detection in Chest CT: A Clinical Investigation Based on the ELCAP Study", Proc. of Second International Workshop on Pulmonary Image Processing in conjunction with MICCAI-09,September 2009, pp. 149-160

[4] Amal Farag, Asem Ali, James Graham, Aly Farag, Salwa Elshazly and Robert Falk, "Evaluation of geometric feature descriptors for detection and classification of lung nodules in low dose ct scans of the chest," International Symposium on Biomedical Imaging (ISBI-11), pp. 169 - 172, Chicago, March 2011.

[5] I. Sluimer, A. Schilham, M. Prokop, and B. van Ginneken, "Computer Analysis of Computed Tomography Scans of the Lung: A Survey," IEEE Transactions on Medical Imaging, vol. 25, No. 4, pp. 385-405, April, 2006.

[6] ELCAP public lung image database - www.via.cornell.edu/databases/lungdb.html

[7] Lee, Y., Hara, T., Fujita, H., Itoh, S., Ishigaki, T, "Automated detection of pulmonary nodules in helical CT images based on an improved template matching technique," IEEE Transactions on Medical Imaging, Vol. 20 pp. 595–604 (2001)

[8] A. Farag, A. El-Baz, G. L. Gimel'farb, R. Falk, M. Abou El-Ghar, T. Eldiasty, S. Elshazly, "Appearance Models for Robust Segmentation of Pulmonary Nodules in 3D LDCT Chest Images," Proc. of International Conference on Medical Image Computing and Computer-Assisted Intervention (MICCAI'06), Copenhagen, Denmark, October 1-6, 2006, pp. 662-670.

[9] A. Farag, J. Graham, A. Farag, S. Elshazly and R. Falk, "Parametric and Non-Parametric Nodule Models: Design and Evaluation", Proc. of Third International Workshop on Pulmonary Image Processing in conjunction with MICCAI-10, September 2010, pp. 151-162

[10] M. B. Stegmann and David Delgado Gomez. A Brief Introduction to Statistical Shape Analysis, Technical University of Denmark, Lyngby, 2002.